Formic Acid Decomposition over Supported Pd Alloy Catalysts: Role of Oxygen in Hydrogen Production

Nandam Hemanth Kumar, † Ankit Kumar, † Riya Javiya, Mukesh Kumar, Sudhanshu Sharma, and Abinaya Sampath*
Indian Institute of Technology Gandhinagar, Palaj, Gujarat, India
*Corresponding author: abinaya.sampath@iitgn.ac.in

Supporting Information

Section S1. Catalyst characterization and experimental method.

Table S1. Catalyst metal loadings, metal particle size distributions, and dispersion over different catalysts.

Catalyst	Pd:Ag bulk molar ratio[a]	Metal loading (%)[a]	Pd:Ag surface molar ratio[b]	Particle size (nm)[c,d]	Particle size (nm)[e,d]	Dispersion (%)[f]	Surface Pd atoms exposed during reaction (mol)[g]
Pd-CeO_2	-	0.9	-	8±3	7 ± 3	15.9	1.3 x 10^{-6}
0.5 PdAg-CeO_2	0.55	0.8	1.46	7±3	7 ± 2	16.3	7.2 x 10^{-7}
Pd-TiO_2	-	1.4	-	6±2	6 ± 2	18.5	2.4 x 10^{-6}
0.5 PdAg -TiO_2	0.44	1.4	NA	7±2	7 ± 2	16.3	1.2 x 10^{-6}
Pd-Al_2O_3	-	0.9	-	13±4	14 ± 5	7.9	6.7 x 10^{-7}
0.5 PdAg-Al_2O_3	0.32	1.5	NA	14±5	12 ± 4	9.5	7.8 x 10^{-7}

[a]Determined by inductively coupled plasma – optical emission spectroscopy (ICP-OES).
[b]Determined by X-ray photoelectron spectroscopy (XPS).
[c]Surface average particle size determined by transmission electron microscopy (TEM) (**Figure 1**).
[d]Standard deviation of particle size distributions determined by TEM.
[e]Number average particle size determined by TEM (**Figure 1).**
[f]calculated from equation 3.
[g]calculated from equation 4.

Surface average particle sizes ($<d_s>$) were calculated using equation 1 and the number average particle sizes ($<d_N>$) were calculated using equation 2.

$$< d_s >= \frac{\sum_{1=i}^{N} d_i^3}{\sum_{1=i}^{N} d_i^2} \qquad (1)$$

$$< d_N >= \frac{1}{N} \sum_{i=1}^{i=N} d_i \qquad (2)$$

where d_i is the measured diameter of nanoparticle *i* and *N* is the total number of nanoparticles measured for any sample. CO chemisorption measurements cannot provide an accurate estimate of the active sites due to the possible adsorption on the supports such as CeO_2 (**Figure 3a**) and TiO_2. The dispersion of the Pd nanoparticles on different monometallic catalysts is calculated by equation 3.[1]

$$D = 6\left(\frac{v}{a}\right) * \left(\frac{1}{< d_N >}\right) \qquad (3)$$

where v is the volume of a Pd atom (0.014 nm^3), a is the surface area of a Pd atom (0.0793 nm^2), and $<d_N>$ is the number average particle size as determined from TEM. The number of the surface Pd atoms on bimetallic catalysts exposed under reaction conditions is difficult to predict due to the dynamic environment. Hence, we assume the Pd to Ag surface molar ratio to be 1.46 based on the XPS measurements on all the alloy catalysts. The ratio assumed provides a higher estimate of the surface Pd atoms as the bulk Pd to Ag molar ratio is ~0.5 as per ICP-OES. The dispersion of the total metal atoms on PdAg catalysts was calculated by weighing the parameters v and a by the molar ratio of Pd and Ag from XPS. Here, the volume of an Ag atom is 0.017 nm^3, and the surface area of an Ag atom is 0.0875 nm^2.

The number of moles of surface Pd on monometallic catalysts is calculated by equation 4.

$$mol\ Pd_s = \frac{D * m}{M_{Pd}} \qquad (4)$$

where m is the bulk metal mass loading in the reactor as measured by ICP-OES, M_{Pd} is the molecular weight of Pd, and D is the dispersion of Pd measured from equation 3. The same equation provides the total number of exposed metal atoms in the alloy catalysts with the molecular weight as the weighted average of molecular weight of Pd and Ag.

Figure S1. Experimental set-up used for FA reaction over different supported Pd catalysts.

Section S2. FA reaction on Pd-CeO_2 and 0.5 PdAg-CeO_2.

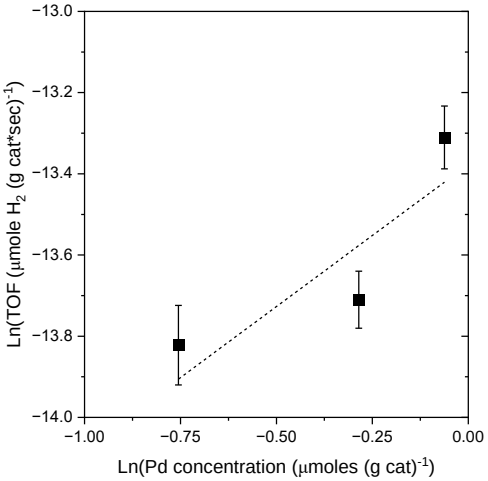

Figure S2. H_2 TOF from FA reaction over Pd-CeO_2 catalysts with different metal loadings of Pd over CeO_2 (100 mg catalyst, 1M FA, 25 mL, 298 K).

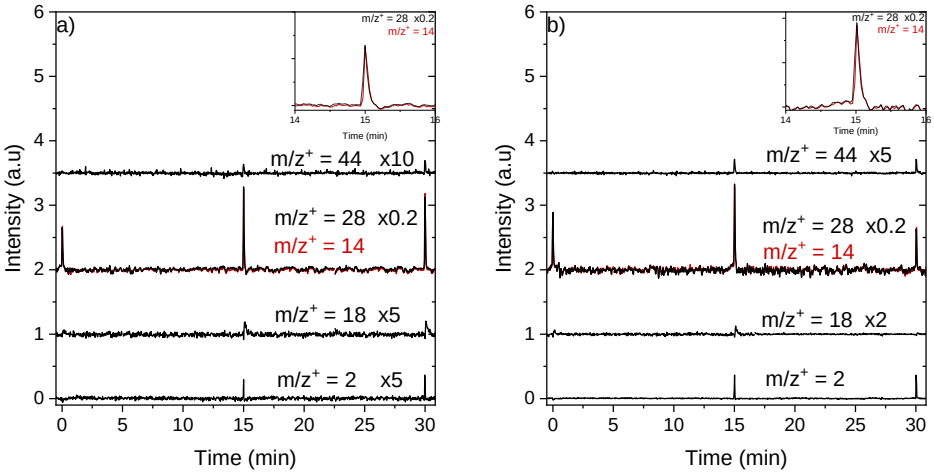

Figure S3. Intensities of mass-to-charge ratios (m/z^+) of 2, 14, 18, 28, and 44 obtained in a mass spectrometer by injecting gaseous products from FA reaction over a) Pd-CeO_2 and b) 0.5 PdAg-CeO_2 at reaction times of 0 minutes, 15 minutes, and 30 minutes. The mass spectrometer uses a carrier gas of a mixture of oxygen and argon (4% oxygen in argon, 22.3 mL min^{-1}, 101 kPa, 298 K). The insets show the m/z^+ of 14 and 28 around the reaction time of 15 minutes.

Fig. S3 shows the mass-to-charge ratios (m/z^+) of 2, 14, 18, 28, and 44 from mass spectrometry of gaseous aliquots from FA reaction over Pd-CeO_2 and 0.5 PdAg-CeO_2 at reaction times of 0 minutes, 15 minutes, and 30 minutes. The mass spectra of pure N_2 shows that the ratio of peak areas of m/z^+ 14 and 28 is 0.2. Based on that data, the peaks around m/z^+ 14 and 28 come from N_2 in the reaction environment at the beginning of the reaction over Pd-CeO_2 and 0.5 PdAg-CeO_2. The gas sample from FA reaction over Pd-CeO_2 and 0.5 PdAg-CeO_2 after 15 minutes of reaction time shows peaks at m/z^+ 2, 14, 18, 28, and 44. The peak at m/z^+ 2 corresponds to H_2 production; 18 corresponds to H_2O formation; 44 corresponds to CO_2 production. However, the ratio of peaks at m/z^+ 14 and 28 is 0.2 (**Fig. S3 insets**), showing that CO production from FA reaction is negligible over Pd-CeO_2 and 0.5 PdAg-CeO_2. We note that the intensity of m/z^+ 2 from FA reaction over 0.5 PdAg-CeO_2 is higher than over Pd-CeO_2, pointing to the higher H_2 TOF over 0.5 PdAg-CeO_2 compared to Pd-CeO_2.

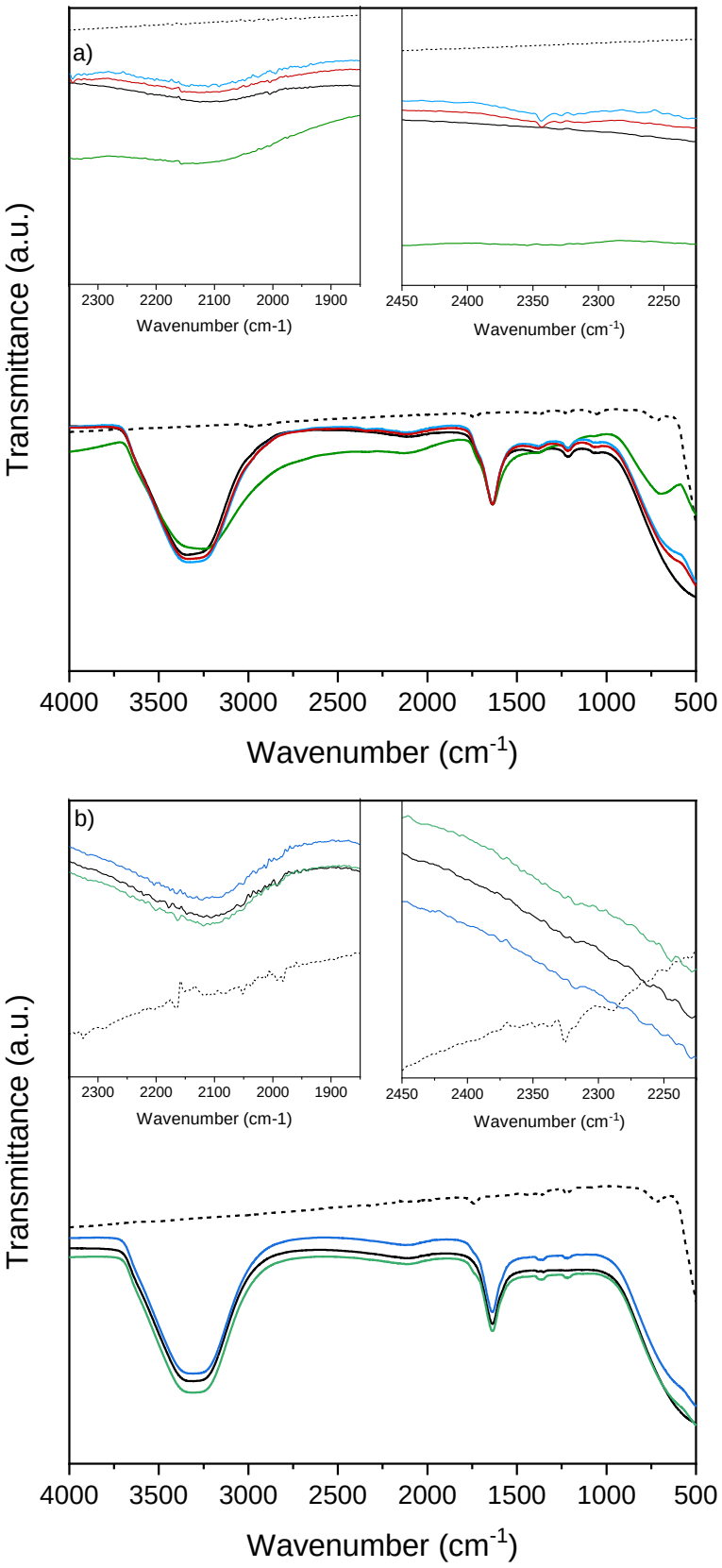

Figure S4. a) Infrared spectra of a mixture of FA and CeO_2 (green), Pd-CeO_2 (blue), 0.5 PdAg-CeO_2 (red); pure FA (black), Pd-CeO_2 (black, dashed) (5 mg catalyst, 1 M FA, 1 mL, 298 K). b) Infrared spectra of the mixture of SF and CeO_2 (green), Pd-CeO_2 (blue); pure SF (black), and Pd-CeO_2 (black, dashed) (5 mg catalyst, 1 M SF, 1 mL, 298 K).

Figure S4a shows the infrared spectra of mixture of FA and CeO_2, Pd-CeO_2 and 0.5 PdAg-CeO_2 against aqueous FA. The infrared spectrum of aqueous FA solution shows peaks around 3340 cm^{-1} and 1640 cm^{-1} that correspond to ν(OH) and δ(H_2O) in H_2O; 1395 cm^{-1} is associated with ν(OCO) in the free formate in bulk.[2, 3] The peak around 2125 cm^{-1} is currently unknown. The peaks at 1217 cm^{-1} and the shoulder at 1720 cm^{-1} originate from the ν(C-O) and ν(C=O) in free FA in the bulk solution or from the CeO_2 framework.[4, 5] Mixture of FA and CeO_2 does not produce any new peaks other than the peaks from aqueous solution. Once FA is added to Pd-CeO_2 and 0.5 PdAg-CeO_2, we see the origin of the peak at 2343 cm^{-1} from CO_2 in the aqueous solution. We do not observe any peaks between 1830 - 2110 cm^{-1} that can be attributed to linear bonded and bridged bonded CO on the Pd surface.[6] The negligible CO production during FA reaction leads to the absence of CO-related features.[7,8,9] To further understand the peaks originating from FA, we performed a control experiment collecting infrared spectra of a mixture of SF and Pd-CeO_2.

Figure S4b shows the infrared spectra of a mixture of SF and CeO_2, and Pd-CeO_2 against aqueous SF. The infrared spectrum of aqueous SF solution shows peaks around 3310 cm^{-1} and 1640 cm^{-1} that correspond to ν(OH) and δ(H_2O) in H_2O; 1350 and 1380 cm^{-1} is associated with the free formate in the bulk.[2] The peak around 2110 cm^{-1} is currently unknown. The peak at 1720 cm^{-1} originates from the FA in the bulk solution of FA and is absent in the aqueous SF solution. A mixture of SF and CeO2 or Pd-CeO_2 produces negligible CO_2 in the aqueous solution. We do not observe any peaks between 1830 - 2110 cm^{-1} that can be attributed to linear bonded and bridged bonded CO on the Pd surface. However, we see two peaks around 1217 cm^{-1} and 1720 cm^{-1} in the mixture of SF and CeO_2/Pd-CeO_2, possibly from the CeO_2 framework.[5, 10]

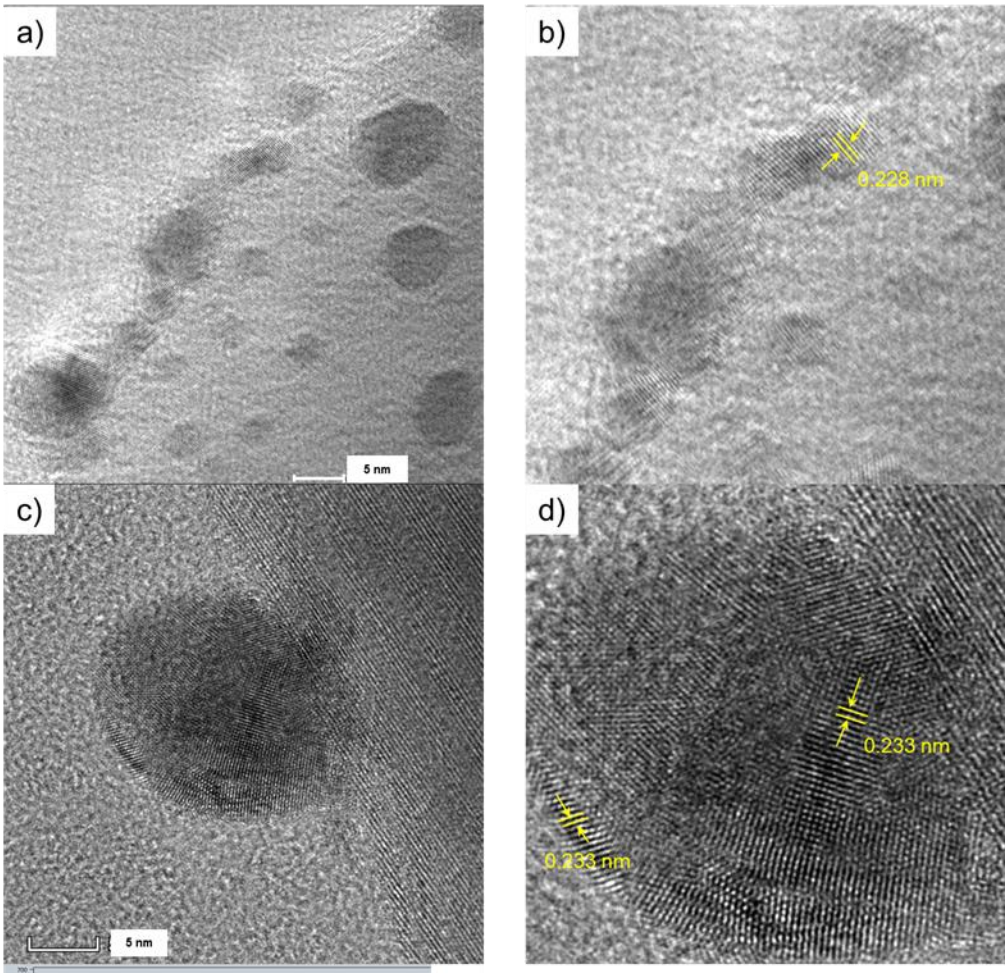

e)

Element	Atomic concentration(%)	Error
Pd	22.62	6.03
Ag	64.94	17.24
Ce	12.44	3.27
O	0.00	19.13

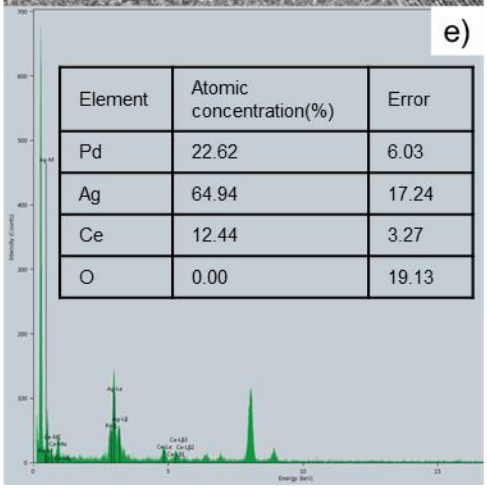

Figure S5. a) Representative high-resolution TEM image of metal particles in Pd-CeO_2 b) Magnified image from part a c) Representative high-resolution TEM image of a metal particle in 0.5 PdAg-CeO_2 d) Magnified image from part c e) Elemental distribution across the image in part c.

Fig. S5a-d show representative high-resolution TEM images of the Pd-CeO_2 and 0.5 PdAg-CeO_2 catalysts. The lattice spacing of 2.28 Å in particles on Pd-CeO_2 corresponds to the Pd (111) plane, whereas an increase in the lattice spacing to 2.33 Å in particles on 0.5 PdAg-CeO_2 indicates the alloying of Pd and Ag in 0.5 PdAg-CeO_2.[11-17] Additionally, the energy dispersive X-ray spectroscopic measurements over the particle in **Fig. S5c** show the presence of both Pd and Ag on the nanoparticle of 0.5 PdAg-CeO_2 catalyst (**Fig. S5e**).

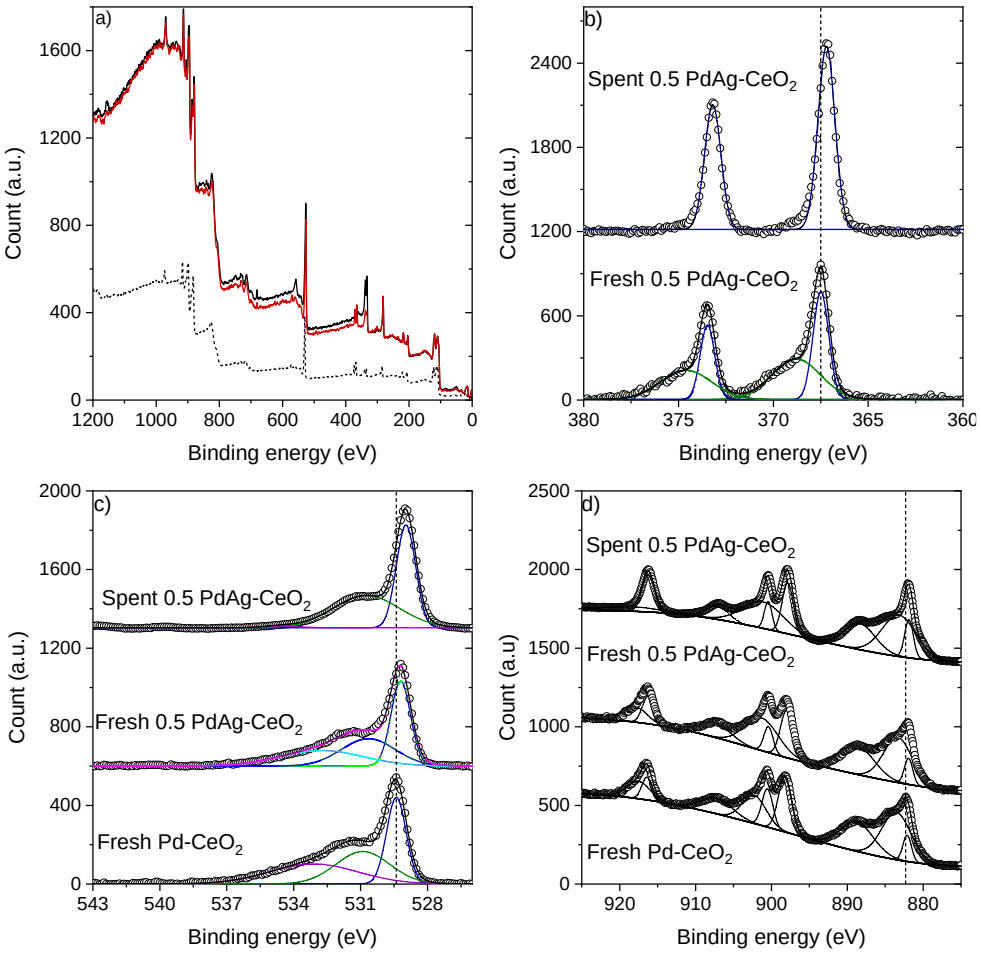

Figure S6. a) XPS spectra of a survey of fresh Pd-CeO_2 (black), fresh 0.5 PdAg-CeO_2 (red), and spent 0.5 PdAg-CeO_2 (dashed) b) XPS spectra of Ag 3d in fresh 0.5 PdAg-CeO_2 and spent 0.5 PdAg-CeO_2 c) XPS spectra of O 1s in fresh Pd-CeO_2, fresh 0.5 PdAg-CeO_2, and spent 0.5 PdAg-CeO_2 d) XPS spectra of Ce 3d in fresh Pd-CeO_2, fresh 0.5 PdAg-CeO_2, and spent 0.5 PdAg-CeO_2 (the open symbols represent the raw data and the solid lines represent Gaussian fits to the data).

Table S2. Peak binding energies of fitted curves of Pd 3d, Ag 3d, O 1s, and Ce 3d spectra along with the percentage surface coverage and surface compositions over fresh Pd-CeO_2, fresh 0.5 PdAg-CeO_2 and spent 0.5 PdAg-CeO_2 surfaces.

Catalyst	Pd $3d_{5/2}$ (eV)		Pd $3d_{3/2}$ (eV)		$Pd^0/(Pd^0 + Pd^{\delta+})$	Ag $3d_{5/2}$ (eV)		Ag $3d_{3/2}$ (eV)		$Ag^0/(Ag^0 + Ag^{\delta+})$	Pd:Ag surface molar ratio
	Pd^0	$Pd^{\delta+}$	Pd^0	$Pd^{\delta+}$		Ag^0	$Ag^{\delta+}$	Ag^0	$Ag^{\delta+}$		
Pd-CeO_2	335.1	336.9	340.3	341.9	0.34	-	-	-	-	-	-
0.5 PdAg-CeO_2	335.3	337.2	340.5	341.8	0.39	367.4	368.8	373.4	374.6	0.45	1.46
0.5 PdAg-CeO_2 (spent)	334.5	336.2	339.8	341.5	0.66	367.2	-	373.1	-	1	0.90
	Ce $3d_{5/2}$ (eV)				Ce $3d_{3/2}$ (eV)					$Ce^{3+}/(Ce^{3+}+Ce^{4+})$	Pd:Ce surface molar ratio
	Ce^{3+}	Ce^{3+}	Ce^{4+}	Ce^{4+}	Ce^{3+}	Ce^{3+}	Ce^{4+}	Ce^{4+}	Ce^{4+}		
Pd-CeO_2	882.1	883.5	888.7	898.2	900.5	902.3	907.2	916.4	917.5	0.48	0.31
0.5 PdAg-CeO_2	881.9	883.3	888.5	897.9	900.4	901.3	907.2	916.2	917.7	0.52	0.14

0.5 PdAg-CeO_2 (spent)	881.9	883.2	888.3	897.8	900.4	901.1	907.1	916.2	918.2	0.57	0.12

	O 1s lattice (eV)	O 1s chemisorbed (eV)	O 1s chemisorbed (eV)	$O_{chem}/(O_{chem}+ O_{latt})$	Ce:O surface molar ratio
Pd-CeO_2	529.4	530.9	533.1	0.67	0.35
0.5 PdAg-CeO_2	529.2	530.6	532.8	0.62	0.38
0.5 PdAg-CeO_2 (spent)	528.9	530.7	534.5	0.54	0.26

Figure S6 shows the *ex situ* XPS spectra of fresh Pd-CeO_2, fresh 0.5 Pd-CeO_2, and spent 0.5 Pd-CeO_2. The survey of the catalysts shows no presence of Ag in Pd-CeO_2 and only features related to atoms of oxygen, Pd, and Ce (**Fig. S6a**). Moreover, the fresh and spent 0.5 PdAg-CeO_2 contains both Pd and Ag. The surface elemental compositions of the catalysts were calculated using the XPS data and the instrument sensitivity factors (**Table S2**). The surface molar ratio of Pd to Ag is 1.46, higher than the bulk molar ratio of ~0.5, hinting at the concentration of Pd at the surface of the fresh 0.5 PdAg-CeO_2. Similarly, the Pd to Ag surface molar ratio is 0.9 in the spent 0.5 PdAg-CeO_2 highlighting that the catalyst surface is more Pd rich than the bulk catalyst during the reaction conditions.

Fig. S6b shows the presence of oxidized Ag (Ag 3d spectrum feature peaks at 368.8 and 374.6 eV) in addition to reduced Ag (Ag 3d spectrum peak at 367.4 and 373.4 eV) on the surface of fresh 0.5 PdAg-CeO_2.[18, 19] However, Ag in the spent 0.5 PdAg-CeO_2 is reduced during the reaction to show Ag 3d peaks at 367.2 eV and 373.1 eV (**Table S2**). **Fig. S6c** shows the O 1s features of fresh Pd-CeO_2, fresh 0.5 Pd-CeO_2, and spent 0.5 Pd-CeO_2. The peak from O 1s in the lattice of CeO_2 (O_{latt}) is around 529.4 eV on fresh Pd-CeO_2 and 529.2 eV on fresh 0.5 PdAg-CeO_2. The surface chemisorbed oxygen (O_{chem}) gives rise to O 1s peaks around 530.9 and 533.1 eV on fresh Pd-CeO_2; 530.6 eV, and 532.8 eV on fresh 0.5 PdAg-CeO_2.[20, 21] The peak areas of different O 1s features show that the surface chemisorbed oxygen reduces from 67% ($O_{chem}/(O_{chem} + O_{latt})$) on fresh Pd-$CeO_2$ to 62% on fresh 0.5 PdAg-CeO_2, possibly due to the modification of Pd-CeO_2 by Ag to provide lower surface coverage of reactive surface oxygen. The XPS spectrum of spent 0.5 PdAg-CeO_2 shows that the surface chemisorbed oxygen reduces to 54%, demonstrating the consumption of surface atomic oxygen during FA reaction (**Table S2**).

Fig. S6d shows the Ce 3d features fresh Pd-CeO_2, fresh 0.5 Pd-CeO_2, and spent 0.5 Pd-CeO_2. **Table S2** shows the peak binding energies of the features from Ce^{3+} and Ce^{4+} in CeO_2.[22] The fresh 0.5 PdAg-CeO_2 provides a higher surface coverage of Ce^{3+} than fresh Pd-CeO_2. The shifts in the O 1s and Ce 3d peaks on 0.5 PdAg-CeO_2 compared to Pd-CeO_2 could be due to the modified interaction of Pd with Ce in the presence of Ag.[23, 24] The spent 0.5 PdAg-CeO_2 provides an even higher surface coverage of reduced Ce (57%) than the fresh 0.5 PdAg-CeO_2 due to the presence of electronically modified Pd and Ag post FA reaction (**Table S2**).

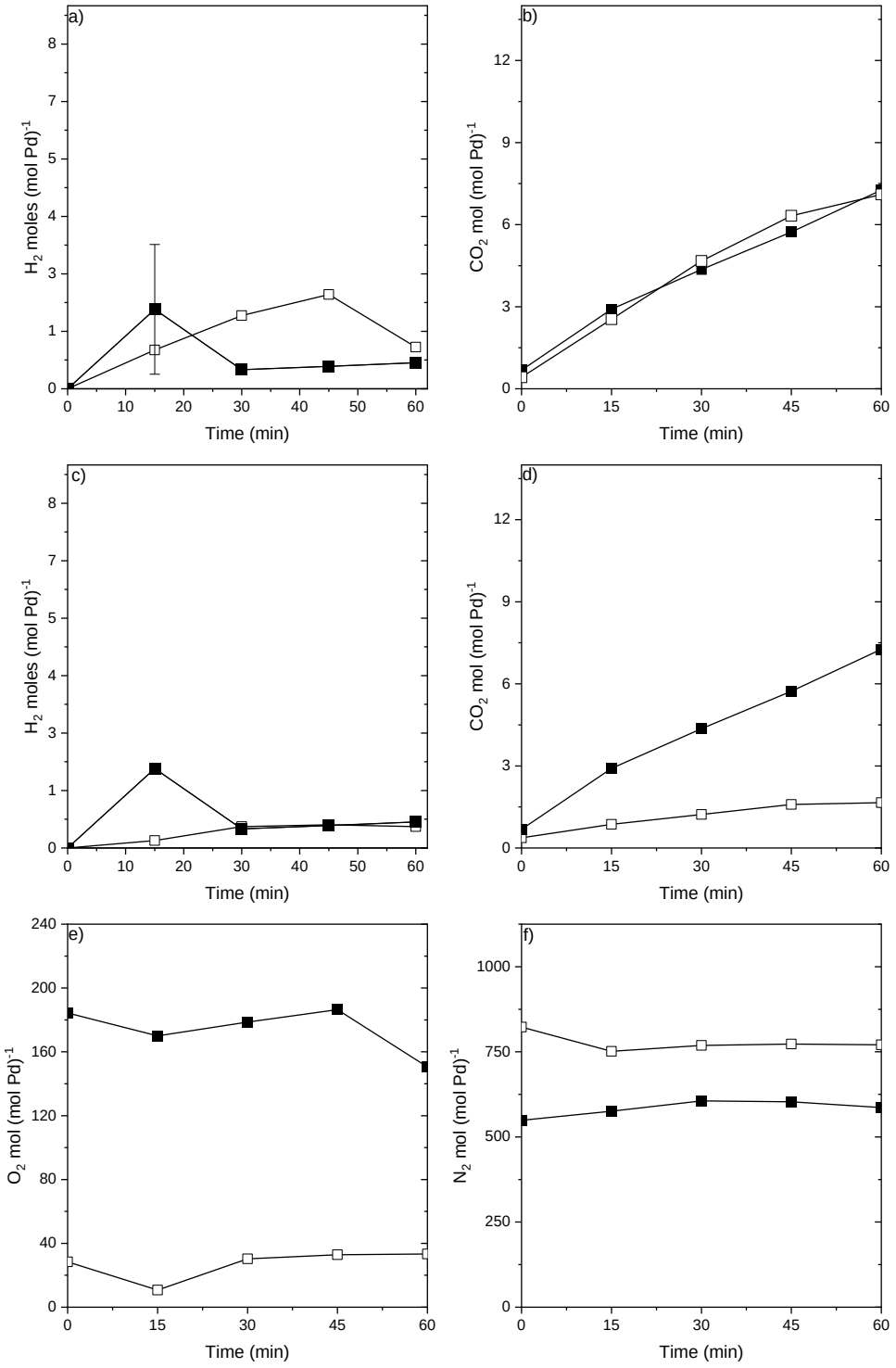

Figure S7. The number of moles of H_2 (a) and CO_2 (b) produced during FA reaction over Pd-CeO_2 (closed) and pre-oxidized Pd-CeO_2 (open) (100 mg catalyst, 25 mL, 1 M FA, 298 K, air in gaseous phase). The number of moles of H_2 (c), CO_2 (d), O_2 (e), and N_2 (f) during the aqueous FA reaction Pd-CeO_2 in the presence of air (closed) and excess N_2 (open) (100 mg catalyst, 25 mL, 1 M FA, 298 K).

Fig. S7a and b show that the oxidized Pd-CeO_2 produce the same H_2 and CO_2 as that of pre-reduced Pd-CeO_2. The exposure of Pd-CeO_2 to ambient conditions before the reaction presents the surface coverage of oxygen on Pd that leads to a negligible difference in the reactivity of Pd-CeO_2 subjected to different pretreatments. FA reaction was carried out in the presence and absence of O_2 in the reaction mixture over Pd-CeO_2 to examine the role of surface oxygen on Pd. **Fig. S7c-S7f** show the number of moles of H_2, CO_2, O_2, and N_2 in contact with the aqueous FA reactant over Pd-CeO_2 in the presence of air. Similar measurements of FA reaction were carried out after purging the air in the reactor with N_2. The purge results in a decrease in the O_2 moles and

an increase in N_2 moles in the gas mixture that is in contact with FA throughout the reaction time, as seen in **Fig. S7e-f**. The decrease in the ambient O_2 results in comparable H_2 production over Pd-CeO_2 from the FA reaction; however, it decreases the amount of CO_2 produced (**Fig. S7c-d**). Pd-CeO_2 activates O_2 in the reaction mixture at ambient temperatures. Hence, a decrease in surface oxygen coverage does not affect the kinetically relevant step in H_2 production from FA but decreases the FA conversion, leading to a decrease in CO_2 production.

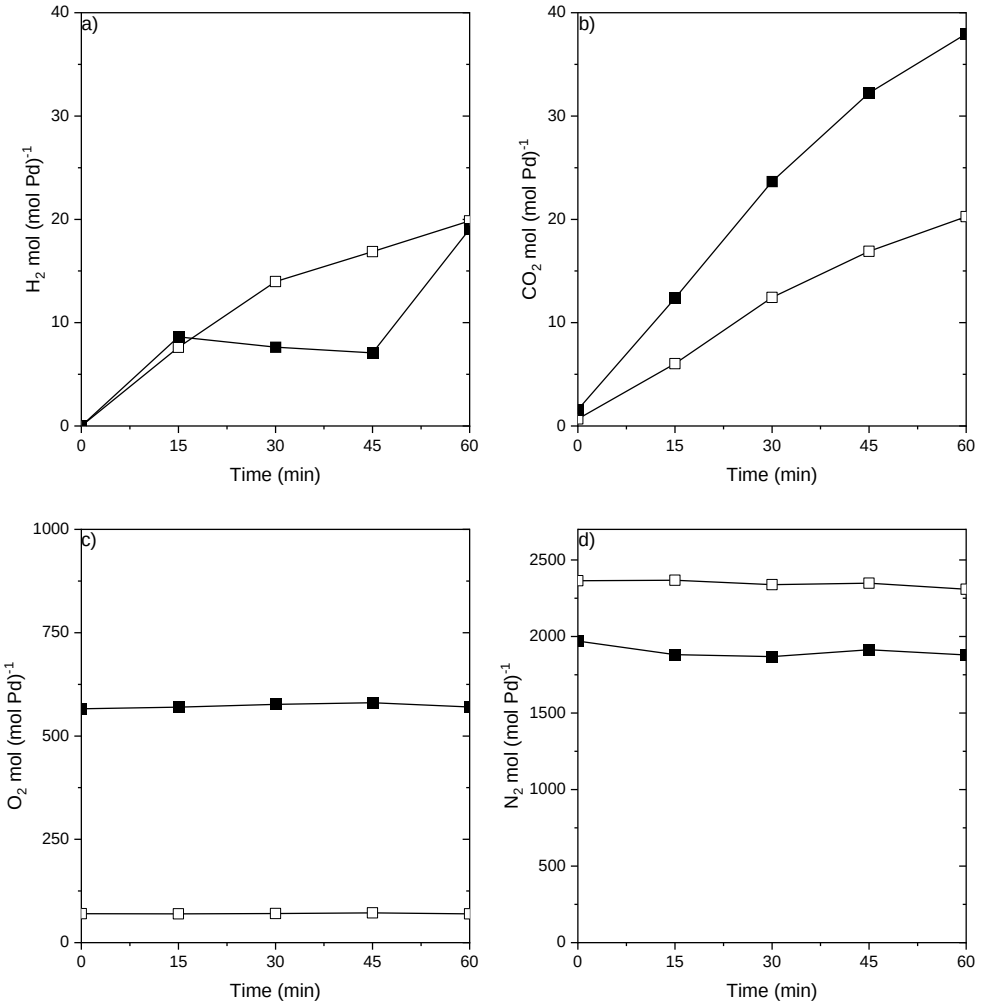

Figure S8. The number of moles of H_2 (a), CO_2 (b), O_2 (c), and N_2 (d) during the aqueous FA reaction 0.5 PdAg-CeO_2 in the presence of air (closed) and excess N_2 (open) (100 mg catalyst, 25 mL, 1 M FA, 298 K).

Fig. S8a-d show the number of moles of H_2, CO_2, O_2, and N_2 in contact with the aqueous FA reactant over 0.5 PdAg-CeO_2 in the presence of air. Similar measurements of FA reaction were carried out after purging the air in the reactor with N_2. The purge results in a decrease in the O_2 moles and an increase in N_2 moles in the gas mixture that is in contact with FA throughout the reaction time, as seen in **Fig. S8c-d**. The decrease in the ambient O_2 results in comparable H_2 production over 0.5 PdAg-CeO_2 from the FA reaction; however, it decreases the amount of CO_2 produced (**Fig. S8a-b**). Therefore, a decrease in surface oxygen coverage does not affect the kinetically relevant step in H_2 production from FA but decreases the FA conversion, leading to a decrease in CO_2 production over 0.5 PdAg-CeO_2, like Pd-CeO_2.

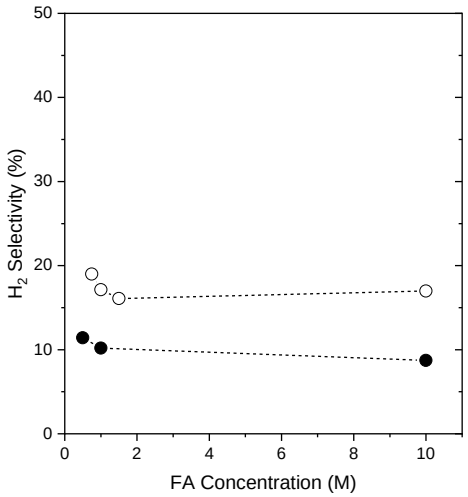

Figure S9. H_2 selectivity as a function of FA concentration over Pd-CeO_2 (filled) and 0.5 PdAg-CeO_2 (empty) (100mg catalyst, 25 mL, 298 K).

Section S3. Proposed mechanism of aqueous FA reaction over Pd-CeO_2 and 0.5 PdAg-CeO_2 catalysts.

Scheme S1. List of proposed elementary steps that occur during aqueous FA reaction over Pd-CeO_2 and 0.5 PdAg-CeO_2 catalysts. $\longrightarrow$ symbol represents an irreversible reaction and $\rightleftharpoons$ represents a reversible elementary step. * represents an empty catalytic site and 'a*' represents a surface adsorbate 'a'.

$HCOOH(aq) \rightleftharpoons HCOO^- + H^+$ - (step 1)

$HCOO^- + 2^* \rightleftharpoons HCOO^* + e^-$ - (step 2)

$HCOO^* + ^* \longrightarrow COO^* + H^*$ - (step 3)

$COO^* \rightleftharpoons CO_2(aq) + 2^*$ - (step 4)

$H^+ + ^* + e^- \rightleftharpoons H^*$ - (step 5)

$H^* + H^* \longrightarrow H_2(aq) + 2^*$ - (step 6)

$H^* + O^* \longrightarrow OH^* + ^*$ - (step 7)

$H^* + OH^* \longrightarrow H_2O^* + ^*$ - (step 8)

$H_2O^* \rightleftharpoons H_2O + ^*$ - (step 9)

$H_2(aq) \rightleftharpoons H_2$ - (step 10)

$CO_2(aq) \rightleftharpoons CO_2$ - (step 11)

$O_2(aq) + 2^* \longrightarrow 2O^*$ - (step 12)

$O_2(aq) \rightleftharpoons O_2$ - (step 13)

The proposed aqueous phase FA reaction mechanism follows **Scheme S1**. The FA dissociates to form formate ($HCOO^-$) and protons (H^+) in the aqueous solution (**step 1**), followed by adsorption of $HCOO^-$ in bidentate adsorption configuration (HCOO*) to delocalize charge over the metal nanoparticle (**step 2**). The C-H bond activation in HCOO* provides the surface-adsorbed CO_2* and H* (**step 3**). The C-H bond activation in surface formate is considered irreversible under the reaction conditions. CO_2* desorbs into the aqueous solution to form the aqueous phase CO_2 ($CO_{2,aq}$) (**step 4**). The protons in the aqueous solution (**step 1**) adsorb to the catalyst surface (H*) upon redistribution of charge density on the catalyst surface with pre-adsorbed HCOO* (**step 5**). Two adsorbed H* atoms undergo associative desorption into aqueous solution ($H_{2,aq}$) (**step 6**). Alternatively, the preexisting surface atomic oxygen (O*) reacts with H* to form surface hydroxyl (OH*) (**step 7**), and the OH* can further react with H* to provide adsorbed water (H_2O*) (**step 8**). H_2O* desorbs into the aqueous solution (**step 9**). The dissolved aqueous H_2, CO_2, and O_2 desorb into the gas phase (**steps 10, 11, and 13).** The consumed O* can be regenerated with irreversible dissociative adsorption of dissolved O_2 **(step 12)**.

The total number of catalytic sites remains conserved and provides equation 5.

$$[L] = [*] + [HCOO*] + [O*] + [COO*] + [H*] + [OH*] + [H_2O*] \qquad (5)$$

where [L] denotes the total number of catalytic sites, [*] represents the total number of empty catalytic sites, [a*] represents the surface concentration of adsorbate 'a'. The rate of step x is given by r_x, k_x represents the forward rate constant of step x, and k_{-x} represents the reverse rate constant of step x. $[H_{2,aq}]$ and $[H_2]$ represent the aqueous and gas phase concentration of H_2, respectively. $[HCOOH]$, $[HCOO^-]$, $[H^+]$, $[O_{2,aq}]$ represent the aqueous phase concentrations of FA, formate, hydrogen ions, and O_2, respectively.

$$r_1 = k_1[HCOOH] - k_{-1}[HCOO^-][H^+] \qquad (6)$$

$$r_2 = \frac{k_2[HCOO^-][*]^2}{[L]} - k_{-2}[HCOO*][e-] \qquad (7)$$

$$r_3 = \frac{k_3[HCOO*][*]}{[L]} \quad (8)$$

$$r_4 = k_4[COO*] - \frac{k_{-4}[CO_2]_{aq}[*]^2}{[L]} \quad (9)$$

$$r_5 = k_5[H^+][*][e-] - k_{-5}[H*] \quad (10)$$

$$r_6 = \frac{k_6[H*]^2}{[L]} \quad (11)$$

$$r_7 = k_7[H*]\frac{[O*]}{[L]} \quad (12)$$

$$r_8 = \frac{k_8[H*][OH*]}{[L]} \quad (13)$$

$$r_9 = k_9[H_2O*] - k_{-9}[H_2O][*] \quad (14)$$

$$r_{12} = \frac{k_{12}[O_{2,aq}][*]^2}{[L]} \quad (15)$$

According to Henry's law,

$$[H_{2,aq}] = k[H_2] \quad (16)$$

Where k is the Henry's constant for H_2 dissolution in H_2O. Substituting equation 16 in equation 11, the rate of formation of gaseous H_2 is given by

$$r_{H2} = \frac{r_6}{k} = \frac{k_6[H*]^2}{k[L]} \quad (17)$$

We assume that steps 1, 2, and 5 are at quasi-equilibrium that results in equations 18, 19, and 20.

$$k_1[HCOOH] = k_{-1}[HCOO^-][H^+] \quad (18)$$

$$\frac{k_2[HCOO^-][*]^2}{[L]} = k_{-2}[HCOO*][e-] \quad (19)$$

$$k_5[H^+][*][e^-] = k_{-5}[H*] \quad (20)$$

Multiplying equations 18, 19, and 20,

$$\frac{k_1k_2k_5[HCOOH]}{[L]} = \frac{k_{-1}k_{-2}k_{-5}[HCOO*][H*]}{[*]^3} \quad (21)$$

We assume the kinetically relevant step for CO_2 formation is step 3. Furthermore, **Fig. S9** shows that the ratio of the rate of H_2 and CO_2 formation is constant across FA concentration, giving the equation 22, where 'a' is a constant.

$$ar_6 = r_3 \quad (22)$$

Substituting equations 8 and 11 in equation 22,

$$a\frac{k_6}{[L]} = \frac{k_3[HCOO*][*]}{[L][H*]^2} \quad (23)$$

Multiplying equation 21 raised to the power -0.4 and equation 23 raised to the power -0.2,

$$\left(\frac{k_1k_2k_5[HCOOH]}{[L]}\right)^{-0.4}\left(a\frac{k_6}{[L]}\right)^{-0.2} = (k_{-1}k_{-2}k_{-5})^{-0.4}\left(\frac{k_3}{[L]}\right)^{-0.2}[HCOO*]^{-0.6}[*] \quad (24)$$

Substituting equation 24 in equation 17,

$$r_{H2} = \frac{r_6}{k} = \frac{r_3}{ak} = \frac{k_3[HCOO*][*]}{ak[L]} = \frac{\frac{k_3}{[L]}[HCOO*]^{1.6}\left(\frac{k_1k_2k_5[HCOOH]}{[L]}\right)^{-0.4}\left(a\frac{k_6}{[L]}\right)^{-0.2}}{ak(k_{-1}k_{-2}k_{-5})^{-0.4}\left(\frac{k_3}{[L]}\right)^{-0.2}} \quad (25)$$

Simplifying equation 25,

$$\frac{r_{H2}}{[L]} = \frac{\frac{k_3}{[L]}[HCOO*]^{1.6}\left(\frac{k_1k_2k_5[HCOOH]}{[L]}\right)^{-0.4}\left(a\frac{k_6}{[L]}\right)^{-0.2}}{ak(k_{-1}k_{-2}k_{-5})^{-0.4}\left(\frac{k_3}{[L]}\right)^{-0.2}[L]} \quad (26)$$

Simplifying equation 26,

$$\frac{r_{H2}}{[L]} = \frac{k_3^{1.2}(k_{-1}k_{-2}k_{-5})^{0.4}([HCOOH])^{-0.4}[HCOO*]^{1.6}}{ak(ak_6)^{0.2}(k_1k_2k_5)^{0.4}[L]^{1.6}} \quad (27)$$

Substituting equation 5 in equation 27,

$$\frac{r_{H2}}{[L]} = \frac{k_3^{1.2}(k_{-1}k_{-2}k_{-5})^{0.4}([HCOOH])^{-0.4}[HCOO*]^{1.6}}{ak(ak_6)^{0.2}(k_1k_2k_5)^{0.4}([*]+[HCOO*]+[O*]+[COO*]+[H*]+[OH*]+[H_2O*])^{1.6}} \quad (28)$$

Assuming [HCOO*] to be the most abundant surface intermediate (MASI), equation 28 simplifies to equation 29.

$$\frac{r_{H2}}{[L]} = \frac{k_3^{1.2}(k_{-1}k_{-2}k_{-5})^{0.4}([HCOOH])^{-0.4}}{a^{1.2}kk_6^{0.2}(k_1k_2k_5)^{0.4}} \quad (29)$$

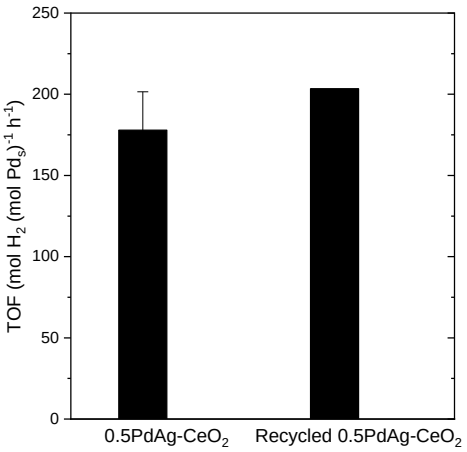

Figure S10. H_2 TOF from FA reaction over 0.5 Pd- Ag-CeO_2 and recycled 0.5 Pd- Ag-CeO_2 (100 mg catalyst, 1 M FA, 25 mL, 298 K).

Section S4. Potentiometric titration of CeO_2 and TiO_2.

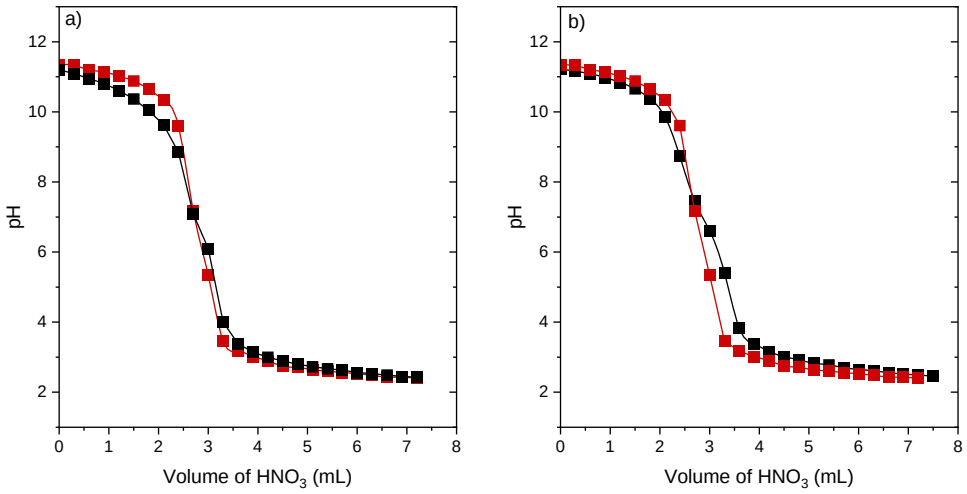

Figure S11. a) Potentiometric titration curves for a suspension of CeO_2 (red) and blank sample (black) were used for the determination of the PZC (1 g CeO_2, 1 M NaOH, 0.1 M HNO_3). b) Potentiometric titration curves for a suspension of TiO_2 (red) and blank sample (black) used for the determination of the PZC (1 g TiO_2, 1 M NaOH, 0.1 M HNO_3).

Section S5. FA reaction on Pd-Al_2O_3 and 0.5 PdAg-Al_2O_3

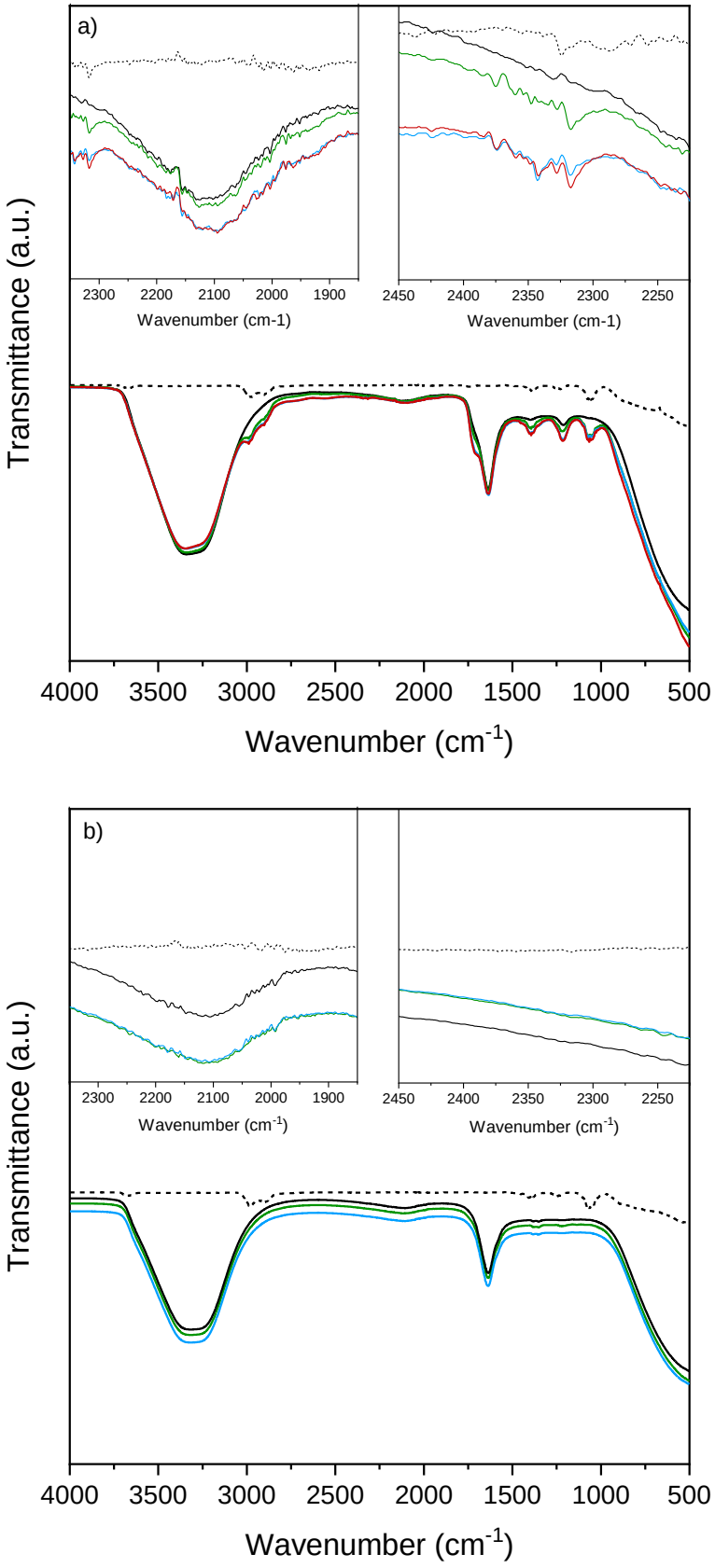

Fig S12. a) Infrared spectra of a mixture of FA and Al_2O_3 (green), Pd-Al_2O_3 (blue), 0.5 PdAg- Al_2O_3 (red); pure FA (black); 0.5 PdAg- Al_2O_3 (black, dashed) (5 mg catalyst, 1 M FA, 1 mL, 298 K). b) Infrared spectra of a mixture of SF and Al_2O_3 (green), Pd-Al_2O_3 (blue); pure SF (black); Pd-Al_2O_3(black, dashed) (5 mg catalyst, 1 M SF, 1 mL, 298 K).

Figure S12a shows the infrared spectra of mixture of FA and Al_2O_3, Pd- Al_2O_3 and 0.5 PdAg- Al_2O_3 against aqueous FA. The infrared spectra of aqueous FA solution show peaks around 3340 cm^{-1} and 1640 cm^{-1} that correspond to ν(OH) and δ(H_2O) in H_2O; 1395 cm^{-1} is associated with ν(OCO) in the free formate in bulk.[2, 3] The peaks around 2125 cm^{-1} are currently unknown. The peaks at 1217 cm^{-1} and the shoulder at 1720 cm^{-1} originate from the ν(C-O) and ν(C=O) in free FA in the bulk solution.[4, 5] A mixture of FA and Al_2O_3 does not produce any new peaks other than the peaks from an aqueous solution of FA and bare Al_2O_3. Once, FA is added to Pd-Al_2O_3 and 0.5 PdAg-Al_2O_3, we see the origin of the peak at 2340 cm^{-1} from CO_2 in the aqueous solution. We do not observe any peaks between 1830 - 2110 cm^{-1} that can be attributed to linear bonded and bridged bonded CO on the Pd surface.[6] The negligible CO production during FA reaction leads to the absence of CO-related features.[7,8,9]

Figure S12b shows the infrared spectra of mixture of SF and Al_2O_3; SF and Pd-Al_2O_3 against aqueous SF. The infrared spectra of aqueous SF solution show peaks around 3310 cm^{-1} and 1640 cm^{-1} that correspond to ν(OH) and δ(H_2O) in H_2O; 1350 and 1380 cm^{-1} are associated with the free formate in the bulk.[2] The peaks around 2120 cm^{-1} are currently unknown. The peak at 1720 cm^{-1} originates from the FA in the bulk solution of FA and is absent in the aqueous SF solution. A mixture of SF and Al_2O_3 or Pd-Al_2O_3 does not produce CO_2 in the aqueous solution. We do not observe any peaks between 1830 - 2110 cm^{-1} that can be attributed to linear bonded and bridged bonded CO on the Pd surface.

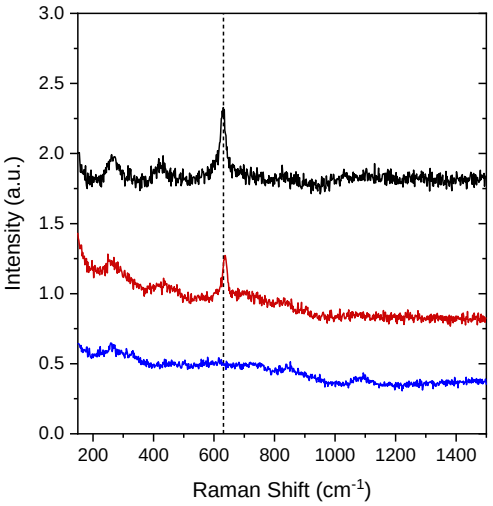

Figure S13. *Ex situ* Raman spectra of Al_2O_3 (blue), Pd-Al_2O_3 (black), 0.5 PdAg-Al_2O_3 (red).

Figure S13 shows the *ex situ* Raman spectra of as prepared Al_2O_3, Pd-Al_2O_3, 0.5 PdAg-Al_2O_3. Raman spectra of Pd-Al_2O_3 and 0.5 PdAg-Al_2O_3 show a sharp feature around 635 cm^{-1} that corresponds to ν(Pd-O).[25-28] Hence, the presence of surface atomic oxygen is observed on both monometallic and bimetallic catalysts on Al_2O_3. The features between 200 – 400 cm^{-1} arise from Al_2O_3.

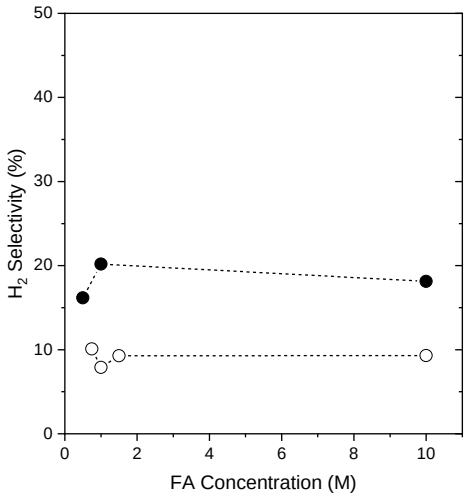

Figure S14. H_2 selectivity as a function of FA concentration over Pd-Al_2O_3 (filled) and 0.5 PdAg-Al_2O_3 (empty) (100mg catalyst, 25 mL, 298 K).

References

1. O. E. Brandt Corstius, J. E. S. van der Hoeven, G. J. Sunley and P. E. de Jongh, *Journal of Catalysis*, 2023, **427**, 115103.
2. L.-Y. Wu, S.-R. Tong, S.-Q. Hou and M.-F. Ge, *The Journal of Physical Chemistry A*, 2012, **116**, 10390-10396.
3. J. Joo, T. Uchida, A. Cuesta, M. T. M. Koper and M. Osawa, *Electrochimica Acta*, 2014, **129**, 127-136.
4. G. Samjeské, A. Miki, S. Ye, A. Yamakata, Y. Mukouyama, H. Okamoto and M. Osawa, *The Journal of Physical Chemistry B*, 2005, **109**, 23509-23516.
5. D. A. Bulushev, M. Zacharska, S. Beloshapkin, Y. Guo and I. Yuranov, *Applied Catalysis A: General*, 2018, **561**, 96-103.
6. P. Xu, F. D. Bernal-Juan and L. Lefferts, *Journal of Catalysis*, 2021, **394**, 342-352.
7. K. Jiang, K. Xu, S. Zou and W.-B. Cai, *Journal of the American Chemical Society*, 2014, **136**, 4861-4864.
8. X. Qin, H. Li, S. Xie, K. Li, T. Jiang, X.-Y. Ma, K. Jiang, Q. Zhang, O. Terasaki, Z. Wu and W.-B. Cai, *ACS Catalysis*, 2020, **10**, 3921-3932.
9. J. Song, S. Bai and Q. Sun, *Colloids and Surfaces A: Physicochemical and Engineering Aspects*, 2023, **658**, 130645.
10. C. Xu and D. W. Goodman, *The Journal of Physical Chemistry*, 1996, **100**, 245-252.
11. L. Karuppasamy, S. Anandan, C.-Y. Chen and J. J. Wu, *Electrocatalysis*, 2017, **8**, 430-441.
12. J. Huang, Q. Liu, Y. Yan, N. Qian, X. Wu, L. Ji, X. Li, J. Li, D. Yang and H. Zhang, *Nanoscale Advances*, 2022, **4**, 111-116.
13. G. Li, X. Wang, X. Zheng, M. Yin, T. Zhang and M. Hei, *ACS Applied Nano Materials*, 2024, **7**, 24082-24092.
14. Z. Yin, Y. Zhang, K. Chen, J. Li, W. Li, P. Tang, H. Zhao, Q. Zhu, X. Bao and D. Ma, *Scientific Reports*, 2014, **4**, 4288.
15. F. Gao, Y. Yin, Z. Cao, H. Li and P. Guo, *Journal of Chemistry*, 2020, **2020**, 1917380.
16. S. A. Bhat, N. Rashid, M. A. Rather, S. A. Pandit, G. M. Rather, P. P. Ingole and M. A. Bhat, *ACS Applied Materials & Interfaces*, 2018, **10**, 16376-16389.
17. Y. Ding, W. Sun, W. Yang and Q. Li, *Applied Catalysis B: Environmental*, 2017, **203**, 372-380.
18. R. N. Lamb, B. Ngamsom, D. L. Trimm, B. Gong, P. L. Silveston and P. Praserthdam, *Applied Catalysis A: General*, 2004, **268**, 43-50.
19. J. Huang, S. Vongehr, S. Tang, H. Lu and X. Meng, *The Journal of Physical Chemistry C*, 2010, **114**, 15005-15010.
20. H. Tan, J. Wang, S. Yu and K. Zhou, *Environmental Science & Technology*, 2015, **49**, 8675-8682.
21. F. Jiang, S. Wang, B. Liu, J. Liu, L. Wang, Y. Xiao, Y. Xu and X. Liu, *ACS Catalysis*, 2020, **10**, 11493-11509.
22. X. Wen, W. Li, J. Yan, X. Wang, E. Ren, Z. Shi, J. Li, X. Ding, S. Mo and D. Mo, *The Journal of Physical Chemistry C*, 2022, **126**, 1450-1461.
23. J. Patarroyo, J. A. Delgado, F. Merkoçi, A. Genç, G. Sauthier, J. Llorca, J. Arbiol, N. G. Bastus, C. Godard, C. Claver and V. Puntes, *Scientific Reports*, 2019, **9**, 18776.
24. H. Wang, S. Luo, M. Zhang, W. Liu, X. Wu and S. Liu, *Journal of Catalysis*, 2018, **368**, 365-378.
25. N. Gao, R. Ma, X. Wang, Z. Jin, S. Hou, W. Xu, Q. Meng, J. Ge, C. Liu and W. Xing, *International Journal of Hydrogen Energy*, 2020, **45**, 17575-17582.
26. G. Xu, J. Liu, Y. Wang, Z. Liu, T. Chen, Y. Yu and H. He, *The Journal of Physical Chemistry C*, 2024, **128**, 2856-2866.
27. A. Baylet, P. Marécot, D. Duprez, P. Castellazzi, G. Groppi and P. Forzatti, *Physical Chemistry Chemical Physics*, 2011, **13**, 4607-4613.
28. S. C. Su, J. N. Carstens and A. T. Bell, *Journal of Catalysis*, 1998, **176**, 125-135.